

CM²



MAGAZINE

第 28 期



南方科技大学海洋磁学中心主编

创刊词

海洋是生命的摇篮，是文明的纽带。地球上最早的生命诞生于海洋，海洋里的生命最终进化成了人类，人类的文化融合又通过海洋得以实现。人因海而兴。

人类对海洋的探索从未停止。从远古时代美丽的神话传说，到麦哲伦的全球航行，再到现代对大洋的科学钻探计划，海洋逐渐从人类敬畏崇拜幻想的精神寄托演变成可以开发利用与科学研究的客观存在。其中，上个世纪与太空探索同步发展的大洋科学钻探计划将人类对海洋的认知推向了崭新的纬度：深海（deep sea）与深时（deep time）。大洋钻探计划让人类知道，奔流不息的大海之下，埋藏的却是亿万年的地球历史。它们记录了地球板块的运动，从而使板块构造学说得到证实；它们记录了地球环境的演变，从而让古海洋学方兴未艾。

在探索海洋的悠久历史中，从大航海时代的导航，到大洋钻探计划中不可或缺的磁性地层学，磁学发挥了不可替代的作用。这不是偶然，因为从微观到宏观，磁性是最基本的物理属性之一，可以说，万物皆有磁性。基于课题组的学科背景和对海洋的理解，我们对海洋的探索以磁学为主要手段，海洋磁学中心因此而生。

海洋磁学中心，简称 CM^2 ，一为其全名“Centre for Marine Magnetism”的缩写，另者恰与爱因斯坦著名的质能方程 $E = MC^2$ 对称，借以表达我们对科学巨匠的敬仰和对科学的不懈追求。

然而科学从来不是单打独斗的产物。我们以磁学为研究海洋的主攻利器，但绝不仅限于磁学。凡与磁学相关的领域均是我们关注的重点。为了跟踪反映国内外地球科学特别是与磁学有关的地球科学领域的最新研究进展，海洋磁学中心特地主办 CM^2 Magazine，以期与各位地球科学工作者相互交流学习、合作共进！

“海洋孕育了生命，联通了世界，促进了发展”。21世纪是海洋科学的时代，由陆向海，让我们携手迈进中国海洋科学的黄金时代

目 录

岩石磁学演绎	2
第 18 章 非磁滞剩磁 ARM.....	2
文献导读	5
1. 下面隐藏着什么?利用橄榄石熔体包裹体重建助长大量硅质火山作用的原始岩浆	5
2. 超慢速扩张 Mohn 脊的热液活动: 近海底磁异常的观测.....	7
3. 古新世-始新世极热期间赤道极热以及浮游生物热应激.....	9
4. 过去千年来中国中部的水汽变化及其与热带太平洋和北大西洋的关系	12
5. 德雷克海峡深水珊瑚记录海冰控制下冰消期深层环流变化.....	16
6. 石笋和考古数据记录的罗马气候适宜期 Tuscany 北部(意大利中部)水文变化	19
7. 黑海东部地壳区域的地球物理综合特征.....	21
8. 伊豆-小笠原-马里亚纳(IBM)弧的基底年龄.....	23

岩石磁学演绎

第 18 章 非磁滞剩磁 ARM

上个世纪,当面对月球上带回的样品时,古地磁学家心里痒痒的,要是能确定样品记录的磁场强度信息,就可以研究月球的月核发电机演化历史,这会是非常大的科学成就!可是,想要精确地确定样品记录的古强度,需要加热样品,但是样品会发生热改变。

当年美国人送给中国极少量的月岩样品,只有小指尖那般大小,比金子贵重不知多少倍。想要烧这些月球岩石样品?门都没有!

既要研究这些珍贵的岩石,又不能烧,古地磁学家沉思,如何解决这个难题?于是,一个类比方案出台了,那就是在实验室的常温下让样品获得非磁滞剩磁 ARM (Rimbert, 1959),它可以模拟 TRM,并避免热处理对样品的影响。

可见 ARM 的提出是为了古地磁学研究。与天然剩磁不同,非磁滞剩磁 (Anhysteresis remanent magnetization, ARM) 是在实验室条件下获得的。随后,ARM 在岩石磁学和环境磁学 (Rock and Environmental Magnetism) 领域被广泛应用。

获得 ARM 需要一个幅度逐渐衰减的交变场 AF (一般 <200 mT) 中,同时需要叠加一个较小的直流场 (DC, 一般为几十 μ T)。这个直流场和地磁场同处一个量级,显而易见是为了模拟地磁场的影响。

ARM 和 TRM 到底有哪些类似的地方呢?

从实验设计来看，其中 AF 退磁过程可以类比于热退磁过程，DC 场的作用与获得 TRM 的外加场作用相同。通过 AF+DC 过程，当交变退磁场的幅值衰减到零时，样品会获得一个与 DC 场呈正比的剩磁 ARM。

和 TRM 一样，ARM 与 DC 场呈正比，所以当 DC 场为零时，其实就是给样品的剩磁进行了系统的 AF 退磁，所以 ARM 也就为零。这种行为就是非磁滞行为，所以把这种剩磁称之为非磁滞剩磁。

交变场 (AF) 可以被看成是一系列连续变化的直流场。AF 的变化具有周期性，其振幅随着时间逐渐衰减到零。当 AF>0 时，样品获得一个正向等温剩磁。在随后的半个周期 AF<0 时，样品会获得一个负向的等温剩磁。只要 AF 的频率足够高，在零场中，样品最后获得的正向磁矩与反向磁矩大小相等，相互抵消，总磁矩为零，从而达到退磁的状态。

根据尼尔理论，

$$\tau = \tau_0 \exp(\mu_0 V M_s H_K / kT * (1 - H_0 / H_K)^2)$$

当存在外场 H_0 时，沿着平行与反平行外场方向的 τ 值不再相等。

假定交变场和直流场分别为 H_{AF} 和 H_{DC} 。在任意时刻，样品所受的外力为 H_{AF} 和 H_{DC} 的矢量和

$$H_0 = H_{AF} + H_{DC}$$

这样，在 AF 的正向期和反向期的 τ 分别为：

$$\tau^+ = \tau_0 \exp \left\{ \frac{K_u V}{kT} \times \left(1 - H_{AF} / H^* + H_{DC} / H^* \right)^2 \right\}$$

$$\tau^- = \tau_0 \exp \left\{ \frac{K_u V}{kT} \times \left(1 - H_{AF} / H^* - H_{DC} / H^* \right)^2 \right\}$$

其中 $H^* = 2K_u / \mu_0 M_s$ 。

通过比较可知，当外场为零时， $\tau^+ = \tau^-$ 。只要时间足够长，SD 颗粒在平行与反平行于易磁化轴的方向具有同等的偏转概率，因而，最终在两个方向上的磁矩大小相等，方向相反，互相抵消。当存在一个向右的外场时，由于 $\tau^+ > \tau^-$ ，这样更多 SD 颗粒的磁矩会沿着外场方向偏转。

通过重复以上的过程时，最终会沿着 H_{DC} 的方向有更多的颗粒偏转。当 AF 逐渐减小后，由于存在能垒的作用下，随意偏转的磁矩也越来越小，其影响可以忽略时，所对应的 H_{AF} 就定义为剩磁的阻挡场 $H_{AF,B}$ (和热剩磁中的阻挡温度类似)。最终样品得到一个不为零的净磁矩，也就是 ARM:

$$ARM = (1/3)\mu_0 M_s \tanh\{(\mu_0 M_s V H_{DC} / kT)(1 - H_{AF,B} / H^*)\}$$

对于弱场，上式可以简化为:

$$ARM = (1/3)\mu_0^2 M_s^2 V H_{DC} (1 - H_{AF,B} / H^*) / kT$$

从上式可知，ARM 与 H_{DC} 呈正比。不同的研究人员会选择不同的 H_{DC} ，造成 ARM 的值无法直接对比。为了消除 H_{DC} 的影响，常常把 ARM 用 H_{DC} 归一化，得到 ARM 磁化率 (χ_{ARM})，其量纲和磁化率的一样，为 $m^3 kg^{-1}$ 。

文献导读

1. 下面隐藏着什么?利用橄榄石熔体包裹体重建助长大量硅质火山作用的原始岩浆



翻译人: 冯婉仪 fengwy@sustech.edu.cn

Barker S J, Rowe M C, Wilson C J N, et al. What lies beneath? Reconstructing the primitive magmas fueling voluminous silicic volcanism using olivine-hosted melt inclusions[J]. Geology, 2020, 48: 504-508.

摘要: 由于原始岩浆通常被滞留在深部, 所以了解驱动大量硅质火山活动发生的地幔熔体的起源具有挑战性。在新西兰的中央 Taupō 火山带 (TVZ) 有一个流纹质火山喷发作用特别强烈的地区。在破火山口流纹质喷发产物中保留有玄武岩-安山岩的痕迹, 它们以包体或火山碎屑的形式保存下来。此外, 部分玄武岩-安山岩出现在破火山口之间的小型单一成因喷发中心。这些镁铁质物质中含有富 MgO 的橄榄石(Fo_{79-86}), 橄榄石中的熔体包裹体捕获了为中央 TVZ 提供补给岩浆的最原始的玄武质熔体。与破火山口有关的 (破火山口内的样品) 橄榄石熔体包裹体的成分不同于与附近的、在破火山口之间出现的镁铁质单一成因喷发中心有关的橄榄石熔体包裹体的成分。来自现代的 Taupō 和 Okataina 破火山口内的熔体包裹体具有更低的不相容元素含量, 这反映出不同的地幔熔体成分。有一个直接的联系表明, 与破火山口有关的硅质火山活动是由玄武质岩浆补给导致的, 这些玄武质岩浆是由更亏损的地幔源区经历更高程度的部分熔融产生的, 并且这些岩浆伴有明显的俯冲特征。Taupō 和 Okataina 火山的位置和活力在根本上是与地幔部分熔融的程度和玄武质岩浆的通量有关, 并且破火山口之间的镁铁质喷发产物不能代表破火山口的补给岩浆。继承的橄榄石及其熔体包裹体提供了一个独特的、驱动活跃的 TVZ 硅质岩浆系统的地幔动力学“窗口”, 并且可能代表了一个能证明其它火山之下存在基性岩浆补给作用的有用方法。

ABSTRACT: Understanding the origins of the mantle melts that drive voluminous silicic volcanism is challenging because primitive magmas are generally trapped at depth. The central Taupō Volcanic Zone (TVZ; New Zealand) hosts an extraordinarily productive region of rhyolitic caldera volcanism. Accompanying and interspersed with the rhyolitic products, there are traces of basalt to andesite preserved as enclaves or pyroclasts in caldera eruption products and occurring as

small monogenetic eruptive centers between calderas. These mafic materials contain MgO-rich olivines (FO_{79-86}) that host melt inclusions capturing the most primitive basaltic melts fueling the central TVZ. Olivine-hosted melt inclusion compositions associated with the caldera volcanoes (intracaldera samples) contrast with those from the nearby, mafic intercaldera monogenetic centers. Intracaldera melt inclusions from the modern caldera volcanoes of Taupō and Okataina have lower abundances of incompatible elements, reflecting distinct mantle melts. There is a direct link showing that caldera-related silicic volcanism is fueled by basaltic magmas that have resulted from higher degrees of partial melting of a more depleted mantle source, along with distinct subduction signatures. The locations and vigor of Taupō and Okataina are fundamentally related to the degree of melting and flux of basalt from the mantle, and intercaldera mafic eruptive products are thus not representative of the feeder magmas for the caldera volcanoes. Inherited olivines and their melt inclusions provide a unique “window” into the mantle dynamics that drive the active TVZ silicic magmatic systems and may present a useful approach at other volcanoes that show evidence for mafic recharge.

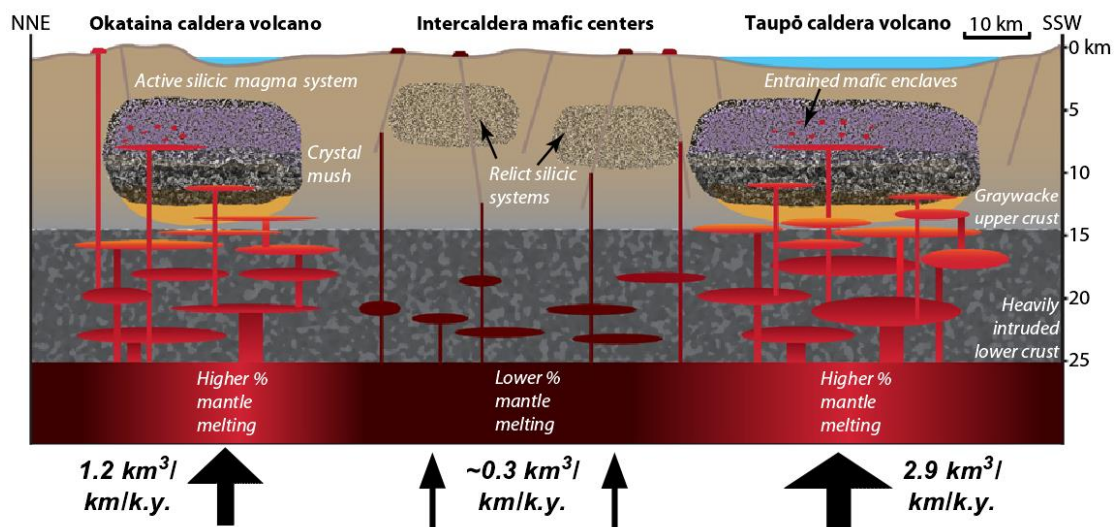


Figure 1. Scaled cross section of crust and upper mantle beneath the central Taupō Volcanic Zone (TVZ, New Zealand), highlighting the contrasts in mantle-melt inputs and crustal pathways to the surface between caldera volcanoes and the intervening sector of the central TVZ. Relict silicic magma systems (active from 350 to 250 ka) refer to those from Gravelly et al. (2016). Magma fluxes across the central TVZ were calculated by considering total heat output from geothermal systems (Bibby et al., 1995) and total eruptive volumes over the past ~60 k.y. (Wilson et al., 2009), assuming that 1 unit volume of rhyolite requires 5× that volume of basalt (see details in Table DR7 [see footnote 1]).

2. 超慢速扩张 Mohn 脊的热液活动：近海底磁异常的观测

翻译人：李园洁 liyj3@sustech.edu.cn



Lim A, Brönnner M, Johansen S E, et al. Hydrothermal Activity at the Ultraslow-Spreading Mohns Ridge: New Insights From Near-Seafloor Magnetics[J]. Geochemistry, Geophysics, Geosystems, 2019, 20(12): 5691-5709.

摘要：热液循环对所有类型的洋中脊是一个基本过程，其很大程度上影响世界海洋的化学和物理平衡。然而，热液点地质环境的多样性使勘探工作复杂化，而且需要对每种情况彻底的研究才能建立有效的标准。综合高分辨率测深和磁测数据的分析,以及视频和岩石样品材料，可帮助我们进一步认识洋中脊热液点，并有助于解释沿轴向火山脊的岩浆和构造过程之间的相互作用。岩石磁数据为解释观测到的洋壳磁化强度变化提供约束。本文绘制出之前发现的活跃的玄武岩型 Loki's Castle 和不活跃的沉积型 Mohn's Treasure 块状硫化物矿床的范围，并推测其地下深度范围。死亡的热液点具有高磁化强度并表现出明显的磁异常特征，容易识别和勾勒。识别出两个死亡热液矿床，MT-2 和 MT-3。Loki's Castle 与穿过矿床的 2 维磁异常剖面观测到的负磁异常一致。在该地区首次的地球物理探测揭示出地质背景的复杂性和地下物理性质的多样性。

ABSTRACT: Hydrothermal circulation is a process fundamental to all types of mid-ocean ridges that largely impacts the chemical and physical balance of the World Ocean. However, diversity of geological settings hosting hydrothermal fields complicates the exploration and requires thorough investigation of each individual case study before effective criteria can be established. Analysis of high-resolution bathymetric and magnetic data, coupled with video and rock samples material, furthers our knowledge about mid-ocean-ridge-hosted venting sites and aid in the interpretation of the interplay between magmatic and tectonic processes along the axial volcanic ridges. The rock-magnetic data provide constraints on the interpretation of the observed contrasts in crustal magnetization. We map the areal extent of the previously discovered active basalt-hosted Loki's Castle and inactive sediment-hosted Mohn's Treasure massive sulfide deposits and infer their subsurface extent. Remarkably, extinct hydrothermal sites have enhanced magnetizations and display clear magnetic signatures allowing their confident identification and delineation. Identified magnetic signatures exert two new fossil hydrothermal deposits, MT-2 and MT-3. The Loki's Castle site coincides with negative magnetic anomaly observed in the 2-D magnetic profile data crossing the deposit. First geophysical investigations in this area reveal the complexity of the geological

setting and the variation of the physical properties in the subsurface.

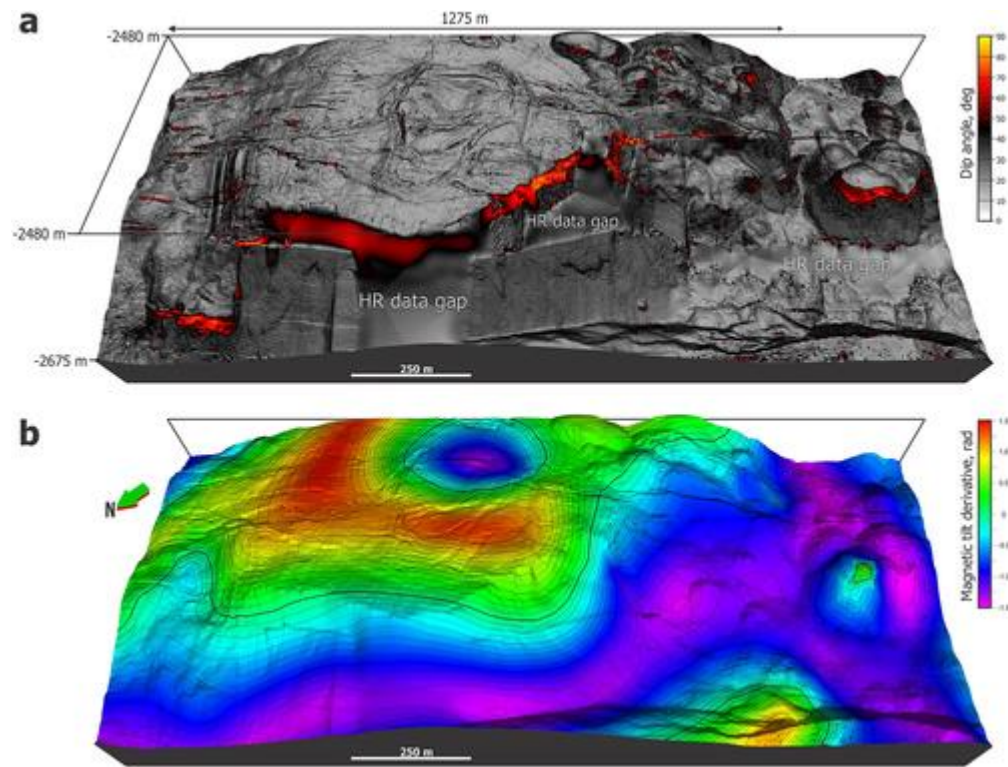


Figure 1. A flat-topped volcano in a 3-D view. (a) Color scheme corresponds to the change in the dip angle. This representation highlights volcanic nature of the topography: flat-topped volcano and its crater, overflowing lava lines, fissures and faults well-resolved at 1 m. High-resolution data gaps are interpolated using minimum curvature algorithm and marked by text. (b) Magnetic Tilt Derivative (TDR) draped onto the bathymetry grid with isolines at 0.1. The thick black line marks zero-crossing.

3. 古新世-始新世极热期间赤道极热以及浮游生物热应激



翻译人：蒋晓东 jiangxd@sustech.edu.cn

Frieling, J., Gebhardt, H., Huber, M. (2017). *Extreme warmth and heat-stressed plankton in the tropics during the Paleocene-Eocene Thermal Maximum*. *Science Advances*. 3(3).

摘要： 在古新世-始新世的极热事件（PETM）期间（~56 Ma），全球海洋温度快速上升约 5 度，热带以外海表温度接近或者超过了现今亚热带温度。基于热带以外温度值，气候模型预测热带海表温度大于 35 度，该值接近许多生物的生理温度。然而很少研究检验所预测的热带高温或者致命性的可能。本研究在尼日利亚的海洋浅水沉积物中识别出 PETM，分析了浮游有孔虫的 Mg/Ca、C 同位素和分子指标 $\text{TEX}^{\text{H}_{86}}$ ，数据表明晚古新世赤道海表温度约为 33 度，并且在 PETM 期间上升到超过 36 度。这一气候模型预测了极地温度放大的尺度并且驳斥了热带恒温的理论。在极热峰值时腰鞭毛虫的丰度和多样性显著降低归因于热应激，这表明快速暖化时热带食物网是易受攻击的。

ABSTRACT: Global ocean temperatures rapidly warmed by $\sim 5^{\circ}\text{C}$ during the Paleocene-Eocene Thermal Maximum (PETM; ~ 56 million years ago). Extratropical sea surface temperatures (SSTs) met or exceeded modern subtropical values. With these warm extratropical temperatures, climate models predict tropical SSTs $>35^{\circ}\text{C}$ —near upper physiological temperature limits for many organisms. However, few data are available to test these projected extreme tropical temperatures or their potential lethality. We identify the PETM in a shallow marine sedimentary section deposited in Nigeria. On the basis of planktonic foraminiferal Mg/Ca and oxygen isotope ratios and the molecular proxy $\text{TEX}^{\text{H}_{86}}$, latest Paleocene equatorial SSTs were $\sim 33^{\circ}\text{C}$, and $\text{TEX}^{\text{H}_{86}}$ indicates that SSTs rose to $>36^{\circ}\text{C}$ during the PETM. This confirms model predictions on the magnitude of polar amplification and refutes the tropical thermostat theory. We attribute a massive drop in dinoflagellate abundance and diversity at peak warmth to thermal stress, showing that the base of tropical food webs is vulnerable to rapid warming.

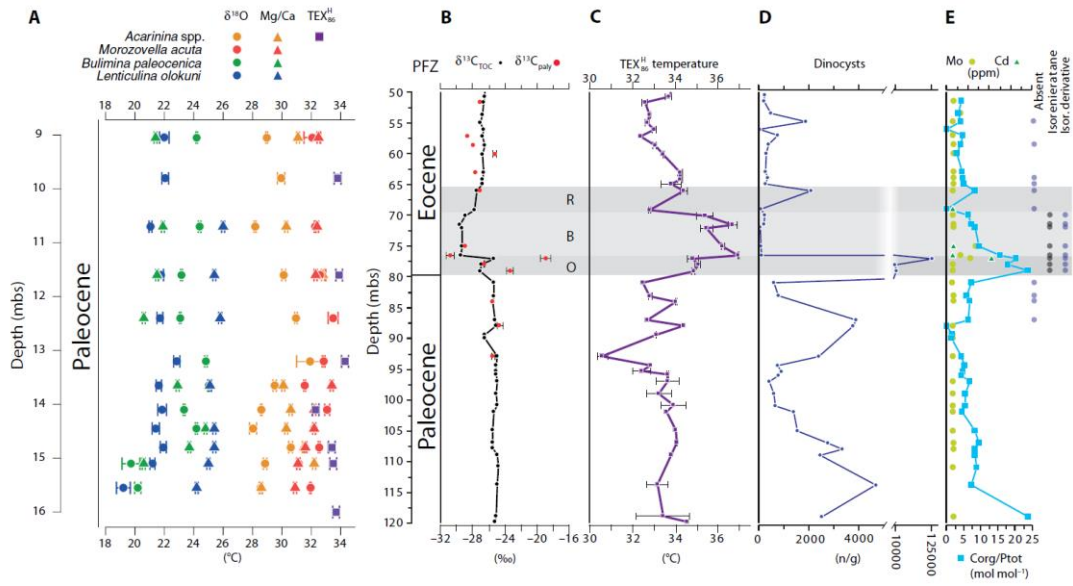


Figure 1. Temperature and environment for the SQ (A) and IB10B core (B to E). (A) SQ surface and bottom-water temperature reconstructions based on Mg/Ca (triangles), $\delta^{18}\text{O}$ (circles) of selected foraminifer species, and $\text{TEX}_{86}^{\text{H}}$ (squares). Error bars represent analytical errors. Conservative 1 σ calibration errors: 1.6°C for $\delta^{18}\text{O}$; 1.7° and 2°C for planktonic and benthic Mg/Ca, respectively; and 2.5°C for $\text{TEX}_{86}^{\text{H}}$. (B) IB10B stable carbon isotope record of TOC ($\delta^{13}\text{C}_{\text{TOC}}$) and palynological residue ($\delta^{13}\text{C}_{\text{paly}}$). The phases of the CIE are denoted by O, B, and R for onset, body, and recovery, respectively. PFZ, planktonic foraminifer zone. (C) $\text{TEX}_{86}^{\text{H}}$ -based SST (error bars based on replicate measurements). (D) Absolute concentrations of dinocysts per gram of dry sediment. Note the scale break between 4,000 and 10,000. (E) Indicators of anoxia: Organic carbon over total phosphorus ratio (Corg/Ptot) (blue squares). Presence of isorenieratene and its derivative. Concentrations of redox-sensitive trace elements Mo (light green circles) and Cd (dark green triangles) in parts per million (ppm). Note that Mo concentrations are close to the detection limit, and absolute values should be treated with caution.

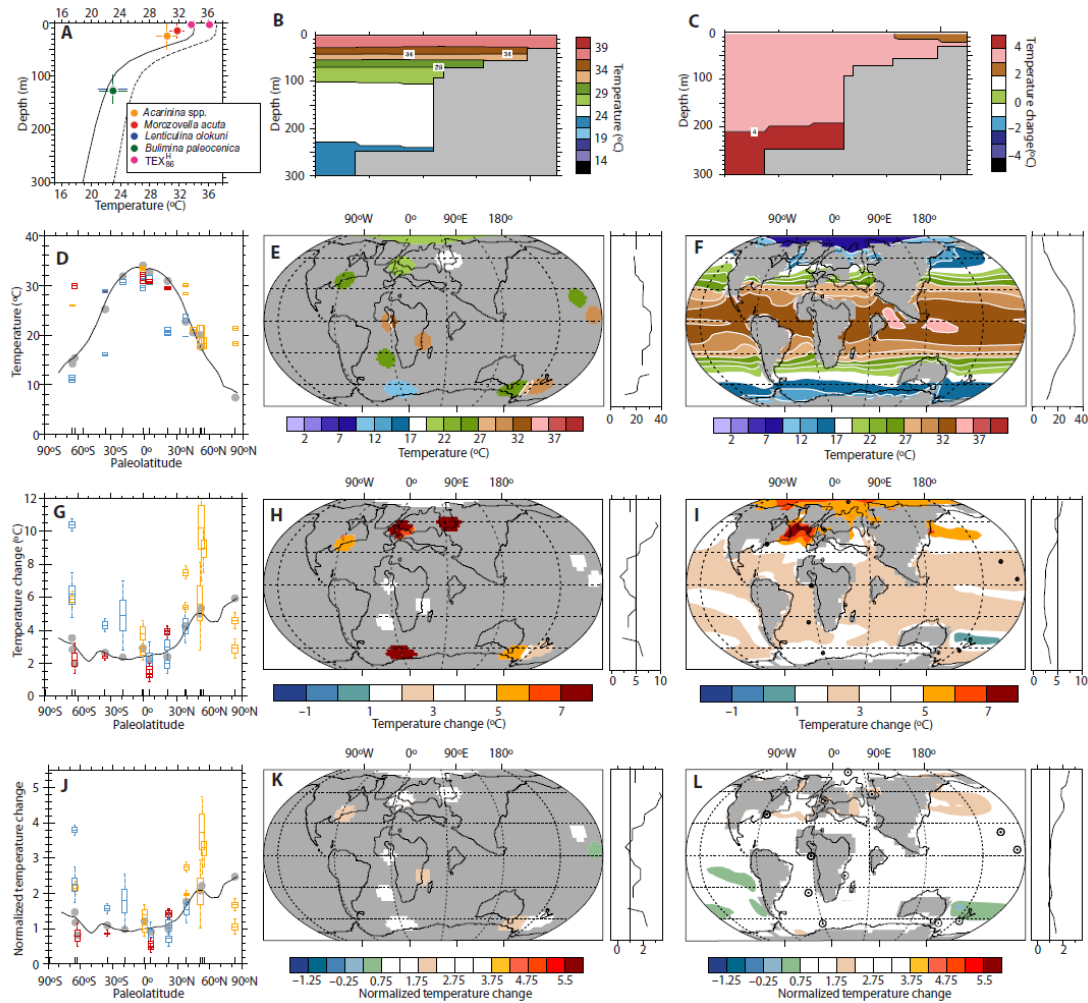


Figure 2. Model-data comparison for latest Paleocene (2240 ppm) and PETM (4480 ppm) CO₂ scenarios. (A) Vertical temperature profile for the site locations. Solid and dashed lines represent latest Paleocene and PETM model estimates, respectively. Data from Fig. 1 (A and C) for comparison, including error bars for depth: *Morozovella* (0 to 30 m), *Acarinina* (0 to 50 m), TEX^H₈₆ (0 m; surface), and benthic (100 to 150 m). (B) Modeled latest Paleocene temperature along an inshore-offshore transect representing the study site. (C) Modeled warming from latest Paleocene to PETM along the same transect. (D) TEX^H₈₆-derived (orange), d¹⁸O-derived (blue), and Mg/Ca-derived (red) SSTs and modeled Paleocene meridional SST gradient (solid line). Gray dots represent point-by-point model-data comparisons. (E) Interpolated absolute SST reconstructions. (F) Modeled latest Paleocene (2240 ppm) temperatures. (G) PETM absolute SST changes and TEX^H₈₆-derived (orange), d¹⁸O-derived (blue), and Mg/Ca-derived (red) SST changes between the latest Paleocene and the PETM. Gray dots represent point-by-point model-data comparisons. (H) Interpolated change in absolute SST. (I) Modeled SST change from the latest Paleocene to the PETM (2240 to 4480 ppm). (J) PETM SST changes, normalized to tropical (20°N to 20°S) SST changes (2.7°C) from the data and TEX^H₈₆-derived (orange), d¹⁸O-derived (blue), and Mg/Ca-derived (red) SST changes between the latest Paleocene and the PETM. Gray dots represent point-by-point model-data comparisons. (K) SST changes from the latest Paleocene to the PETM from the data, normalized to tropical SST changes in the data (2.7°C). (L) SST changes from the latest Paleocene to the PETM, normalized to tropical SST changes in CESM1 (2.4°C). Black circles indicate site locations.

4. 过去千年来中国中部的水汽变化及其与热带太平洋和北大西洋的关系



翻译人: 杨会会 11849590@mail.sustech.edu.cn

Duan F C, Zhang Z Q, Wang Y et al. *Hydrological variations in central China over the past millennium and their links to the tropical Pacific and North Atlantic oceans*[J]. *The Climate of the Past*, 2019, 16: 475-485

摘要: 东亚夏季风主导的降雨(又称梅雨)在过去千年的变化,有助于启发未来变暖气候下水汽的变化。本文提供了一个来自中国中部永兴洞的,具有高分辨率且能精准定年的石笋 $\delta^{18}\text{O}$ 记录。结合之前发表的同一洞穴的记录,我们的新记录表明梅雨的变化与全球气温变化有关。特别地,我们的记录显示,梅雨在中世纪气候异常期(MCA)期间减弱,而在小冰期(LIA)期间增强。在目前的暖期(CWP),我们的记录显示梅雨也有类似的减弱。此外,在MCA和CWP期间,我们的记录显示,中国北方的大气降水同样湿润,中部的大气降水同样干燥,但在CWP期间,中国南方的大气降水相对湿润。这种空间差异表明了区域降水对人为作用的复杂局部响应。在MCA(LIA)期间减弱(增强)的梅雨与北半球表面气温的暖(冷)相吻合。这种梅雨模式也很符合热带印度-太平洋暖池区的气候条件。另一方面,我们的记录也显示了与北大西洋气候的紧密联系。梅雨的减少(增加)与北大西洋振荡的正(负)相有很好的相关性。另外,我们的记录与MCA(LIA)期间大西洋经向翻转环流的强(弱)有很好的联系。所有上述提及的十年-百年尺度上的区域响应和遥相关,指示梅雨与MCA和LIA期间热带太平洋和北大西洋的海洋过程密切相关。

ABSTRACT: Variations of precipitation, also called the Meiyu rain, in the East Asian summer monsoon (EASM) domain during the last millennium could help enlighten the hydrological response to future global warming. Here we present a precisely dated and highly resolved stalagmite $\delta^{18}\text{O}$ record from the Yongxing Cave, central China. Our new record, combined with a previously published one from the same cave, indicates that the Meiyu rain has changed dramatically in association with the global temperature change. In particular, our record shows that the Meiyu rain was weakened during the Medieval Climate Anomaly (MCA) but intensified during the Little Ice Age (LIA). During the Current Warm Period (CWP), our record indicates a similar weakening of

the Meiyu rain. Furthermore, during the MCA and CWP, our records show that the atmospheric precipitation is similarly wet in northern China and similarly dry in central China, but relatively wet during the CWP in southern China. This spatial discrepancy indicates a complicated localized response of the regional precipitation to the anthropogenic forcing. The weakened (intensified) Meiyu rain during the MCA (LIA) matches well with the warm (cold) phases of Northern Hemisphere surface air temperature. This Meiyu rain pattern also corresponds well to the climatic conditions over the tropical Indo-Pacific warm pool. On the other hand, our record shows a strong association with the North Atlantic climate as well. The reduced (increased) Meiyu rain correlates well with positive (negative) phases of the North Atlantic Oscillation. In addition, our record links well to the strong (weak) Atlantic meridional overturning circulation during the MCA (LIA) period. All abovementioned localized correspondences and remote teleconnections on decadal to centennial timescales indicate that the Meiyu rain was coupled closely with oceanic processes in the tropical Pacific and North Atlantic oceans during the MCA and LIA.

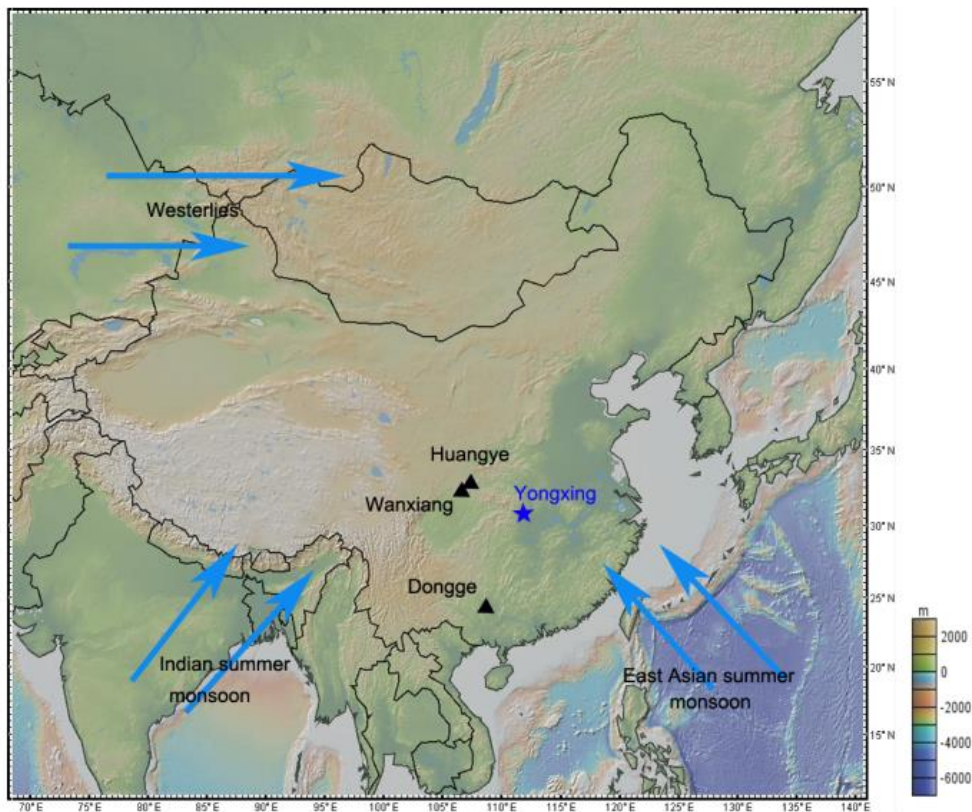


Figure 1. A schematic climate setup of East Asian monsoon systems and our study site. This figure was made with GeoMapApp (<http://www.geomapapp.org>, last access: 12 January 2020). The blue star and black triangles represent Yongxing Cave in central China and other caves in the monsoonal region, respectively.

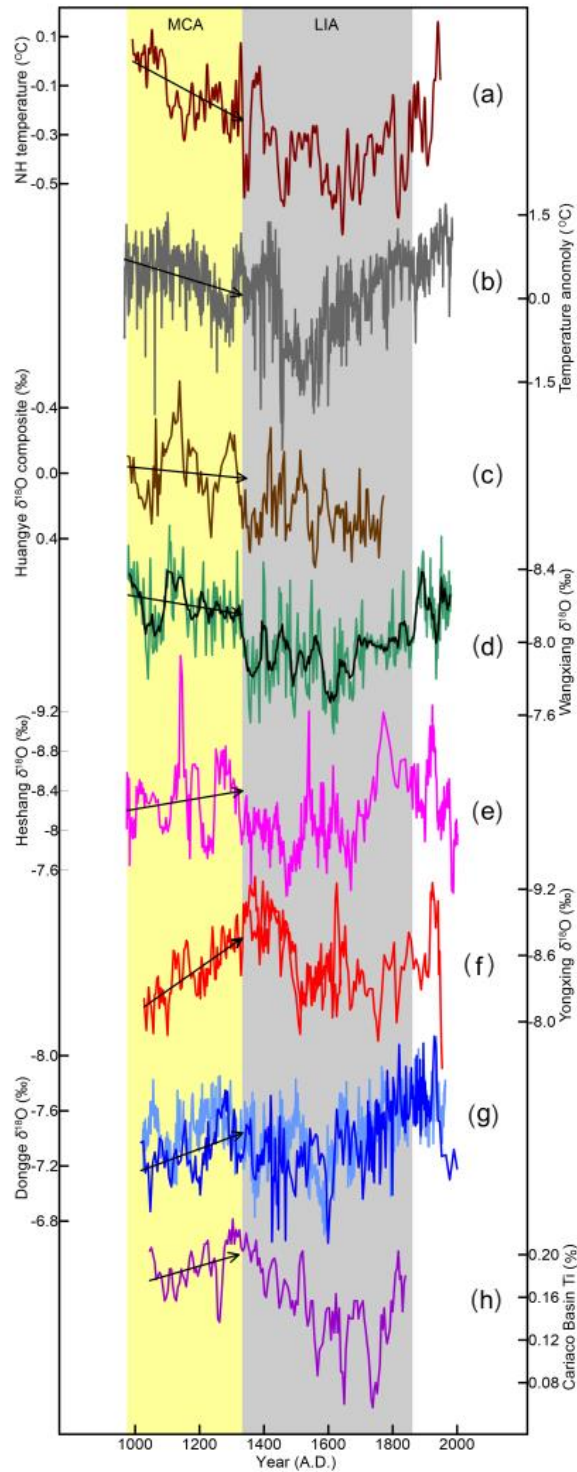


Figure 2. A comparison of the Yongxing $\delta^{18}\text{O}$ time series with other proxy records. (a) Northern Hemisphere reconstructed temperature (Mann et al., 2009); (b) northern China reconstructed temperature (Tan et al., 2003); (c) Huangye Cave $\delta^{18}\text{O}$ composite (Tan et al., 2011b); (d) Wanxiang Cave $\delta^{18}\text{O}$ record (Zhang et al., 2008); (e) Heshang Cave $\delta^{18}\text{O}$ record (Hu et al., 2008); (f) Yongxing Cave record (this study); (g) Dongge Cave record (Wang et al., 2005; Zhao et al., 2015); (h) Cariaco Basin Ti content record (Haug et al., 2001). Light yellow and blue bars indicate the MCA and LIA, respectively. Arrows, constrained by linear fit methods, indicate trends of the climatic variations.

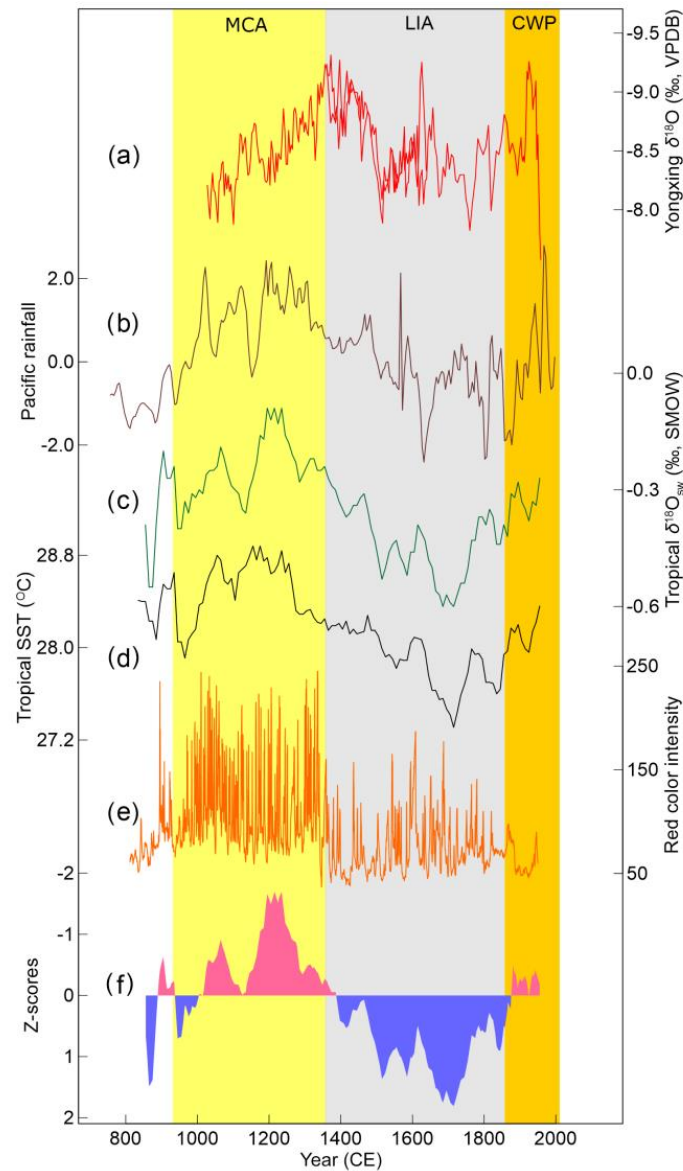


Figure 3. A comparison between Meiyu rain and Pacific climate. **(a)** Yongxing Cave record (this study); **(b)** tropical Pacific rainfall record (Oppo et al., 2009); **(c)** tropical Pacific $\delta^{18}\text{O}$ record (Oppo et al., 2009); **(d)** tropical Pacific sea surface temperature (Oppo et al., 2009); **(e)** red color intensity in southern Ecuador (Moy et al., 2002); **(f)** hydrological reconstruction of ENSO from the tropical Pacific (Yan et al., 2011a). Yellow, grey, and orange bands represent the MCA, LIA, and CWP, respectively.

5. 德雷克海峡深水珊瑚记录海冰控制下冰消期深层环流变化



翻译人：仲义 zhongyi@sustech.edu.cn

David J. Wilson, Torben Struve, Tina van de Flierdt, et al., *Sea-ice control on deglacial lower cell circulation changes recorded by Drake Passage deep-sea corals [J]. Earth and Planetary Science Letters*, 2020, 544, 116405. <https://doi.org/10.1016/j.epsl.2020.116405>

摘要：末次冰消期和全新世之间的深海环流连续性变化为理解末次冰消期以来气候变化一共提供了重要依据，同时其变化对于理解深海在全球碳循环的过程具有重要影响。尽管我们已经知道在冰期时大量的碳被埋藏在深海翻转流之中，而在冰消期时被释放出来，但是这些变化的机制还仍未解决。南大洋海冰在调控全球大洋分层和环流以及碳埋藏过程中发挥重要作用，但是验证这一概念模型需要更多指示洋流变化的数据来支撑。因此，作者首次展示了来自德雷克海峡下部绕极深层水的冷水珊瑚中钕（Nd）同位素记录，结果显示冰消期有 2.5 ϵNd 的变化，末次盛冰期 ϵNd 更加偏正达到 -5.9，说明这一时期分层作用增强，有限的北大西洋海水中 Nd 进入下部绕极深层水中；而在冰消期时，在 Heinrich 1 早期大西洋深层水开始增强，影响南大洋深层水，该事件也对应于南极海冰后撤，随后在南极短暂变冷时期（Antarctic Cold Reversal, ACR）结果更偏向太平洋海域端元。这些变化证明南大洋环流对于深海环流重要控制作用，同时也进一步支持海冰对于深海水团结构的影响。因此，通过对南大洋下部绕极深层水(LCDW)的 Nd 同位素研究，我们的结果对于其他海盆冰消期环流特征变化提供重要解释，同时支持北大西洋深层水金鱼大西洋深水东南部和西南部存在空间不一致性的差异。

ABSTRACT: The sequence of deep ocean circulation changes between the Last Glacial Maximum and the Holocene provides important insights for understanding deglacial climate change and the role of the deep ocean in the global carbon cycle. Although it is known that significant amounts of carbon were sequestered in a deep overturning cell during glacial periods and released during deglaciation, the driving mechanisms for these changes remain unresolved. Southern Ocean sea-ice has recently been proposed to play a critical role in setting the global deep ocean stratification and circulation, and hence carbon storage, but testing such conceptual and modelling studies requires data constraining past circulation changes. To this end, we present the first deglacial dataset of neodymium (Nd) isotopes measured on absolute-dated

deep-sea corals from modern Lower Circumpolar Deep Water depths in the Drake Passage. Our record demonstrates deglacial variability of 2.5 ϵNd units, with radiogenic values of up to $\epsilon\text{Nd} = -5.9$ during the Last Glacial Maximum providing evidence for a stratified glacial circulation mode with restricted incorporation of Nd from North Atlantic Deep Water in the lower cell. During the deglaciation, a renewed Atlantic influence in the deep Southern Ocean is recorded early in Heinrich Stadial 1, coincident with Antarctic sea-ice retreat, and is followed by a brief return to more Pacific-like values during the Antarctic Cold Reversal. These changes demonstrate a strong influence of Southern Ocean processes in setting deep ocean circulation and support the proposed sea-ice control on deep ocean structure. Furthermore, by constraining the Nd isotopic composition of Lower Circumpolar Deep Water in the Southern Ocean, our new data are important for interpreting deglacial circulation changes in other ocean basins and support a spatially asynchronous return of North Atlantic Deep Water to the deep southeast and southwest Atlantic Ocean.

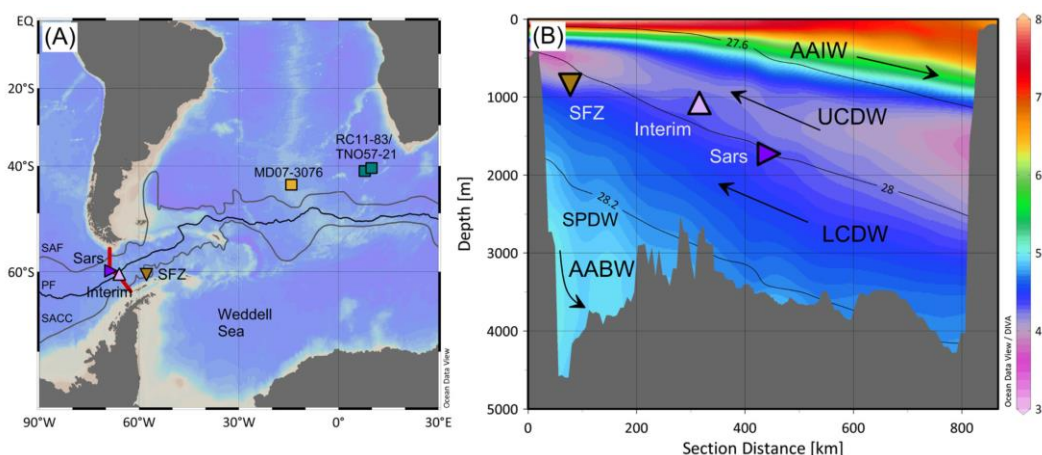


Figure 1. Location map and hydrographic section across the Drake Passage. (a) Location of the Drake Passage coral samples and South Atlantic sediment cores from the Cape Basin (RC11-83/TNO57-21; Piotrowski et al., 2008, 2012) and Mid-Atlantic Ridge (MD07-3076; Skinner et al., 2013). Also shown are mean positions of the surface fronts of the ACC (Orsi et al., 1995): SAF, Subantarctic Front; PF, Polar Front; SACC, Southern ACC Front. SFZ, Shackleton Fracture Zone. (b) Section across the Drake Passage showing oxygen in ml/l (coloured; Garcia et al., 2014), neutral density anomaly in kgm^{-3} (black contour lines; Jackett and McDougall, 1997), and sub-surface water masses (Rintoul et al., 2001; Sudre et al., 2011). AAIW, Antarctic Intermediate Water; UCDW, Upper Circumpolar Deep Water; LCDW, Lower Circumpolar Deep Water; SPDW, Southeast Pacific Deep Water; AABW, Antarctic Bottom Water. (For interpretation of the colours in the figure(s), the reader is referred to the web version of this article.)

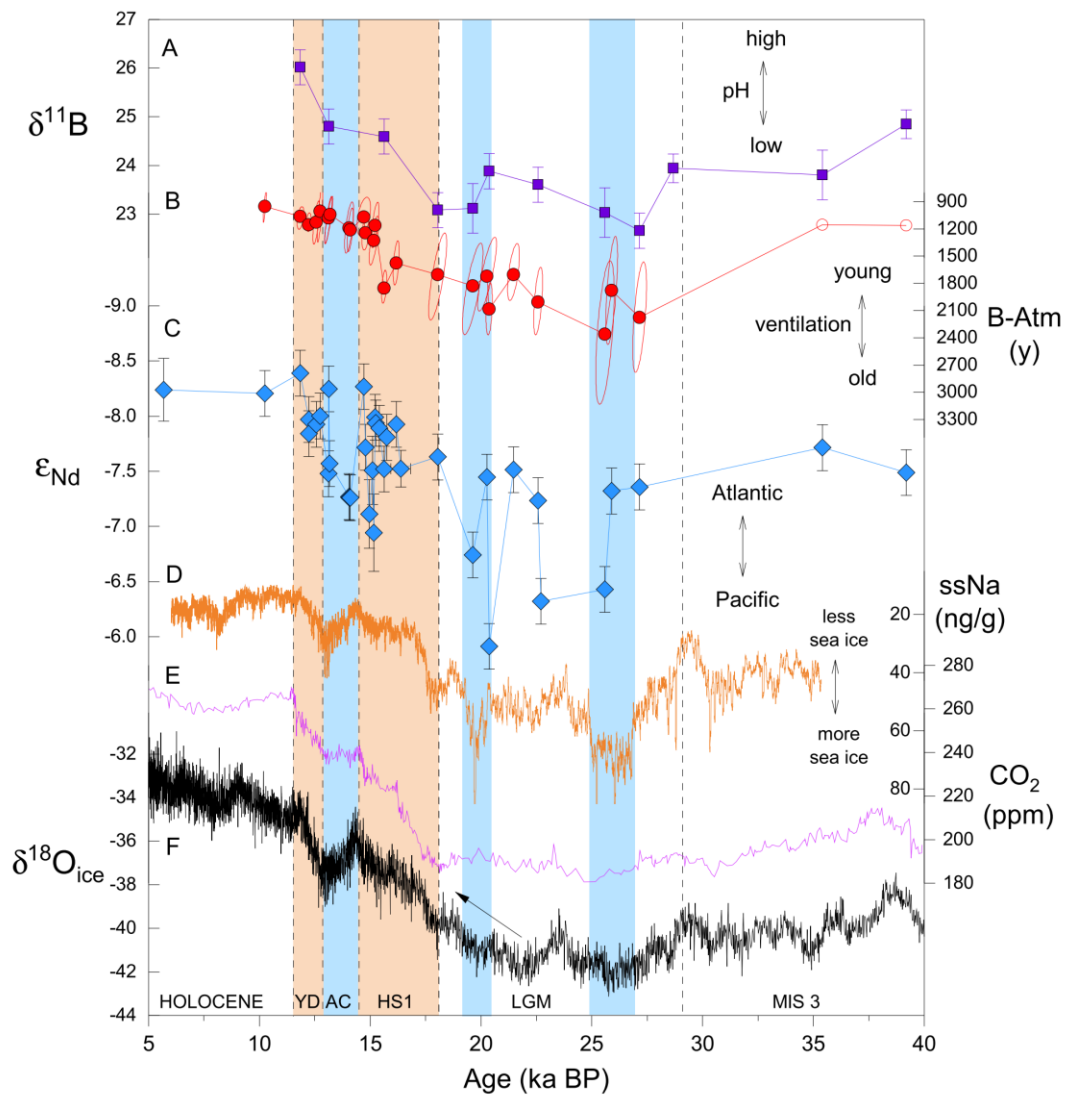


Figure 2. Evolution of water mass sourcing and chemical properties of LCDW from 5 to 40 ka, based on Drake Passage deep-sea corals, compared to Southern Ocean climate records. (a) Deep water pH inferred from boron isotopes (Rae et al., 2018). (b) Deep water radiocarbon age offset from the contemporaneous atmosphere (B-Atm) (Burke and Robinson, 2012; Chen et al., 2015). Open symbols indicate two samples with large uncertainties in B-Atm and for clarity their error ellipses ($\pm \sim 2$ -2.5 kyr) are not shown. (c) Neodymium isotopes in LCDW corals (uncertainties for Nd isotopes are 2SD; uncertainties for ages are smaller than the symbol size). (d) Sea-salt sodium (ssNa, 15-point smoothed) in WAIS Divide Core as a proxy for sea-ice extent (WAIS Divide Project Members, 2015). (e) Atmospheric CO₂ compilation from Antarctic ice cores (Bereiter et al., 2015). (f) Antarctic temperature proxy $\delta^{18}\text{O}_{\text{ice}}$ in WAIS Divide Core (WAIS Divide Project Members, 2015), with arrow indicating early deglacial warming. Blue bars highlight the Antarctic Cold Reversal and two intervals during the LGM with particularly expanded sea-ice, which each correspond to shifts towards more radiogenic Nd isotopes. Orange bars highlight Antarctic warm intervals during the deglaciation. YD, Younger Dryas; AC, Antarctic Cold Reversal; HS1, Heinrich Stadial 1; LGM, Last Glacial Maximum; MIS 3, Marine Isotope Stage 3.

6. 石笋和考古数据记录的罗马气候适宜期 Tuscany 北部（意大利中部）水文变化



翻译人：郑威 11930589@mail.sustech.edu.cn

Bini M, Zanchetta G, Regattieri E, et al. Hydrological changes during the Roman Climatic Optimum in northern Tuscany (Central Italy) as evidenced by speleothem records and archaeological data[J]. Journal of Quaternary Science, 2020.

摘要：地中海盆地不同历史时期的气候变化研究对于人类居住模式的演化十分重要。虽然罗马时代一直以来被认为处于一个气候适宜期，但是最近的研究表明区域性气候变化仍然十分复杂。本文，作者对比石笋代用指标记录的水文变化和根据Tuscany北部的考古遗址记录重建的洪水记录。作者发现了在公元前1世纪有一个气候震荡的时期，终结于一个几十年的干旱事件，在随后的一个世纪，降雨增加，那时罗马帝国刚刚兴起，然后，在公元2世纪重新回到干旱的条件。石笋记录的降雨增加的时期与考古发现的洪水记录和历史洪水数据对应良好。这些数据表明在公元3-4世纪该地区又重新回到湿润的条件。

ABSTRACT: Study of the climate in the Mediterranean basin during different historical periods has taken on a particular importance, particularly regarding its role (together with other factors) in the evolution of human settlement patterns. Although the Roman age is traditionally considered a period with a favourable climate, recent studies have revealed considerable complexity in terms of regional climate variations. In this paper, we compare the hydrological change from speleothem proxy records with flood reconstructions from archaeological sites for Northern Tuscany (central Italy). We identify a period of oscillating climatic conditions culminating in a multidecadal dry event during the 1st century BC, followed by a century of increased precipitation at the beginning of the Roman Empire and subsequently a return to drier conditions in the 2nd century AD. The period of rainfall increase documented by the speleothems agrees with both the archaeological flood record as well as historical flood data available for the Tiber River, ca. 300 km to the south. These data also suggest a return to wetter conditions following the 3rd and 4th centuries AD.

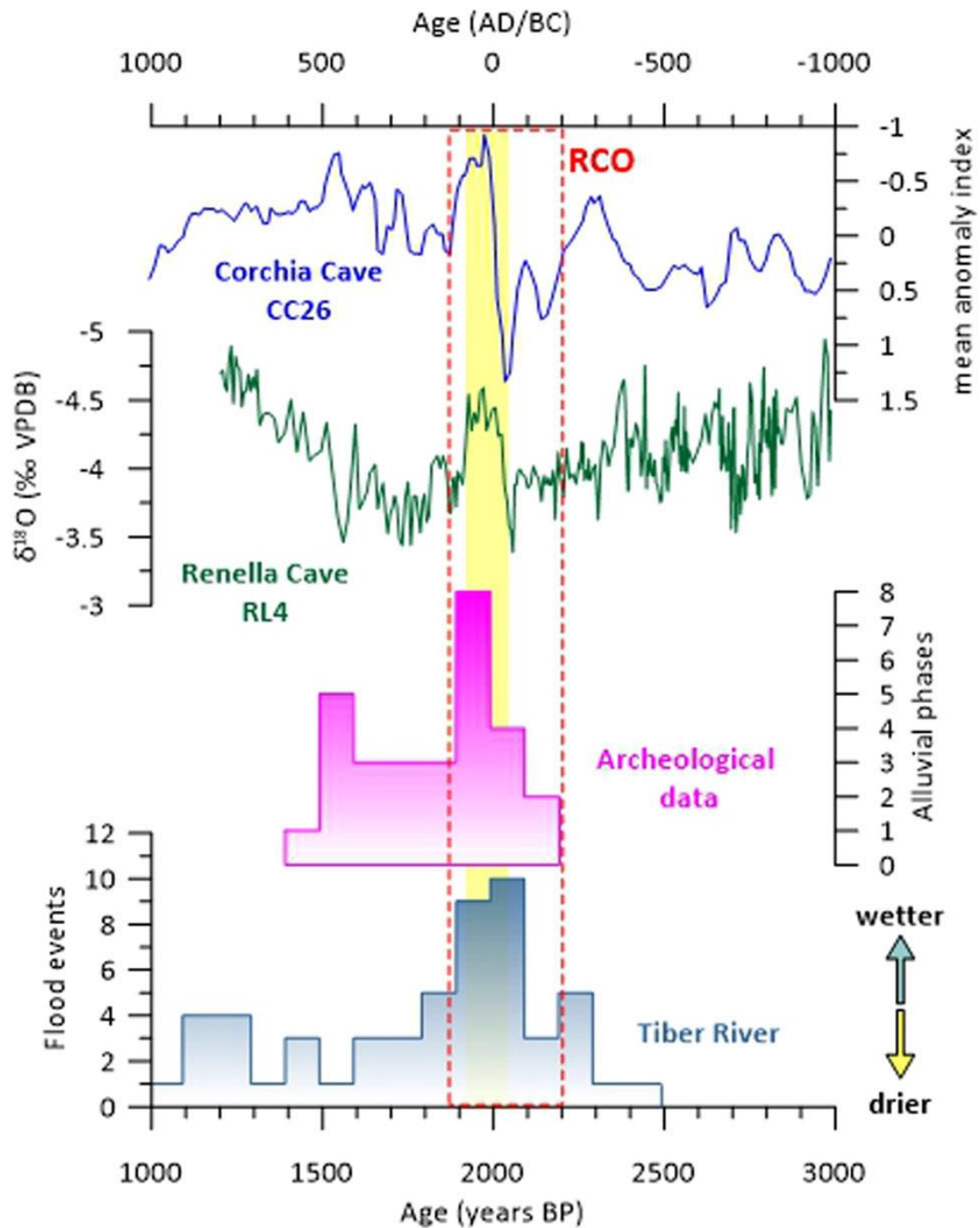


Figure 1. RL4 and CC26 records compared with floods inferred from archaeological data (source Table 1) and Tiber River flood historical records (data from Aldrete, 2007). The chronology of floods obtained from the archaeological data were spread over a century. This can produce some differences between the number of floods between Table 1 and this figure. This has no impact on the spike during the 1st century A

7. 黑海东部地壳区域的地球物理综合特征



翻译人：曹伟

Monteleone V, Minshull T A, Marinmoreno H, et al. *Integrated geophysical characterization of crustal domains in the eastern Black Sea*[J]. *Geology*, 2020. <https://doi.org/10.1130/G47056.1>

摘要：裂谷作用可能最终导致大陆分裂，但由此产生地壳分布的识别与表征仍然存在争议。此外，岩浆分裂作用的时空变化可能会影响新形成洋壳的地球物理特征，从而导致对地壳组成和分布的不同解释。在黑海东部盆地(EBSB)，从裂陷到裂解的演化过程一直是争论的话题，对于延伸的陆壳和洋壳分布有多种解释。我们从长偏移距地震反射剖面解释基底形态的变化，突出显示了从西北向东南的断裂和倾斜大陆块体到粗糙而平滑的基底过渡。我们对磁异常进行建模进一步约束不同基底区域，并推断在西北部存在弱磁化、延伸的陆壳，以及与中部和东南部平滑基底一致的0.4–3.8 A/m层位。我们通过地壳厚度和地壳速度的突变推断，EBSB洋壳向西北方向延伸的更远。这些不同类型的地球物理证据之间的明显差异可能是由于裂解期间岩浆供应的变化，从而影响到所形成洋壳的厚度和速度结构。

ABSTRACT: Rifting may lead ultimately to continental breakup, but the identification and characterization of the resulting crustal distribution remains challenging. Also, spatial and temporal changes in breakup magmatism may affect the geophysical character of the newly formed oceanic crust, resulting in contrasting interpretations of crustal composition and distribution. In the Eastern Black Sea Basin (EBSB), the evolution from rifting to breakup has been long debated, with several interpretations for the distribution of stretched continental and oceanic crust. We interpret basement morphological variations from long-offset seismic reflection profiles, highlighting a northwest-to-southeast transition from faulted and tilted continental blocks to a rough and then smoother basement. We model magnetic anomalies to further constrain the various basement domains, and infer the presence of a weakly magnetized, stretched continental crust in the northwest, and a 0.4–3.8 A/m layer coinciding with the smooth basement in the central and southeastern area. We conclude that the EBSB oceanic crust extends farther to the northwest than was suggested previously from an abrupt change in crustal thickness and lower-crustal velocity. The apparent discrepancy between these different types of geophysical evidence may result from changes in magma supply during breakup, affecting the thickness and velocity structure of the resulting oceanic crust.

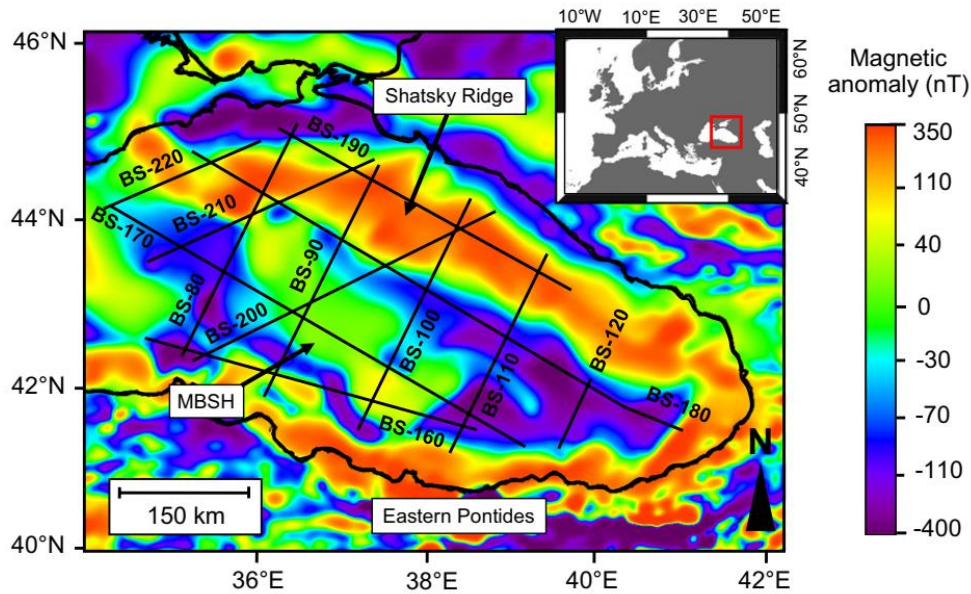


Figure 1. Reduced-to-pole magnetic anomaly map (Earth Magnetic Anomaly Grid, EMAG2v3, <https://www.ngdc.noaa.gov/geomag/emag2.html>; Meyer et al., 2017) for the Eastern Black Sea Basin region. Black lines mark Geology Without Limits Group (www.gwl-geo.com) seismic profiles. Prominent positive anomalies correspond to Shatsky Ridge, mid-Black Sea high (MBSH), Eastern Pontides magmatic arc, and contrast with the negative anomaly of the central basin.

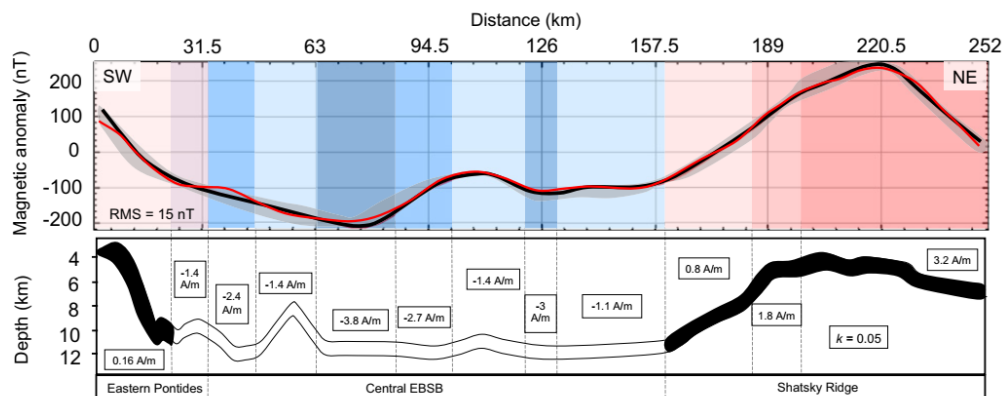


Figure 2. Magnetic anomaly modeling along profile BS-110 (location shown in Figs. 1 and 2A). Top panel displays a comparison between calculated (red line) and observed (black line) anomalies. Root-mean-squared (RMS) error between observed and calculated anomaly is shown at the bottom left corner. Gray band represents anomaly variations 15 km to either side of the profile. Colored backgrounds show the lateral extent and intensity (dark—high intensity; pale—low intensity) of magnetized layers: pink—continental domain; blue—oceanic crust. Bottom panel shows model generating calculated anomaly and magnetization for each layer. The source of the magnetic anomalies was assumed to lie within a 1-km-thick layer with the given intensity of magnetization (in A/m). Black blocks are normally magnetized. The susceptibility (k) value used for the continental crust also is shown. EBSB—Eastern Black Sea Basin.

8. 伊豆—小笠原—马里亚纳(IBM)弧的基底年龄



翻译人: 刘伟 inewway@163.com

Ishizuka O, Hickeyvargas R, Arculus R J, et al. Age of Izu-Bonin-Mariana arc basement[J]. Earth and Planetary Science Letters, 2018: 80-90.

摘要: 厘清西太平洋伊豆—小笠原—马里亚纳(IBM)弧系统的早期构造和岩浆演化, 对于理解太平洋和菲律宾海板块在汇聚背景下的俯冲起始过程和原因至关重要。弧前火成岩剖面为海底扩张始于在 52 Ma (俯冲开始的时间)和产生“弧前玄武岩”提供了有力证据。IODP 351 航次在 Amami Sankaku Basin (ASB) 收获了低 Ti 拉斑玄武岩地壳, 其在俯冲开始后不久形成, 位于未来 IBM 弧远端(名义上的弧后地区)。这一基底的放射测年显示的年龄范围(49.3-46.8 Ma, 加权平均值为 48.7 Ma)与现今 IBM 弧前的玄武岩相重叠, 但比弧前玄武岩活动开始时要年轻 3.3 Ma。弧后玄武岩和弧前玄武岩在年龄范围和地球化学特征上的相似性表明, 在俯冲启动过程中由海底扩张形成的新洋壳从现今 IBM 弧的弧前延伸到弧后。考虑到最古老的弧前玄武岩与 ASB 地壳的年龄差异, 可能发生了洋脊跃迁引起的不对称扩张。这一 ASB 形成的情形表明, 在俯冲起始阶段, Daito 脊的中生代残余弧构成了仰冲板块。相较于下沉板块和仰冲板块都是海洋板块的情况, 相对轻的残余弧与海洋板块相邻的情况更有利于俯冲的开始。

ABSTRACT: Documenting the early tectonic and magmatic evolution of the Izu–Bonin–Mariana (IBM) arc system in the Western Pacific is critical for understanding the process and cause of subduction initiation along the current convergent margin between the Pacific and Philippine Sea plates. Forearc igneous sections provide firm evidence for seafloor spreading at the time of subduction initiation (52 Ma) and production of “forearc basalt”. Ocean floor drilling (International Ocean Discovery Program Expedition 351) recovered basement-forming, low-Ti tholeiitic basalt crust formed shortly after subduction initiation but distal from the convergent margin (nominally reararc) of the future IBM arc (Amami Sankaku Basin: ASB). Radiometric dating of this basement gives an age range (49.3–46.8 Ma with a weighted average of 48.7 Ma) that overlaps that of basalt in the present-day IBM forearc, but up to 3.3 m.y. younger than the onset of forearc basalt activity. Similarity in age range and geochemical character between the reararc and forearc basalts implies that the ocean crust newly formed by seafloor spreading during subduction initiation extends from

fore- to reararc of the present-day IBM arc. Given the age difference between the oldest forearc basalt and the ASB crust, asymmetric spreading caused by ridge migration might have taken place. This scenario for the formation of the ASB implies that the Mesozoic remnant arc terrane of the Daito Ridges comprised the overriding plate at subduction initiation. The juxtaposition of a relatively buoyant remnant arc terrane adjacent to an oceanic plate was more favourable for subduction initiation than would have been the case if both downgoing and overriding plates had been oceanic.

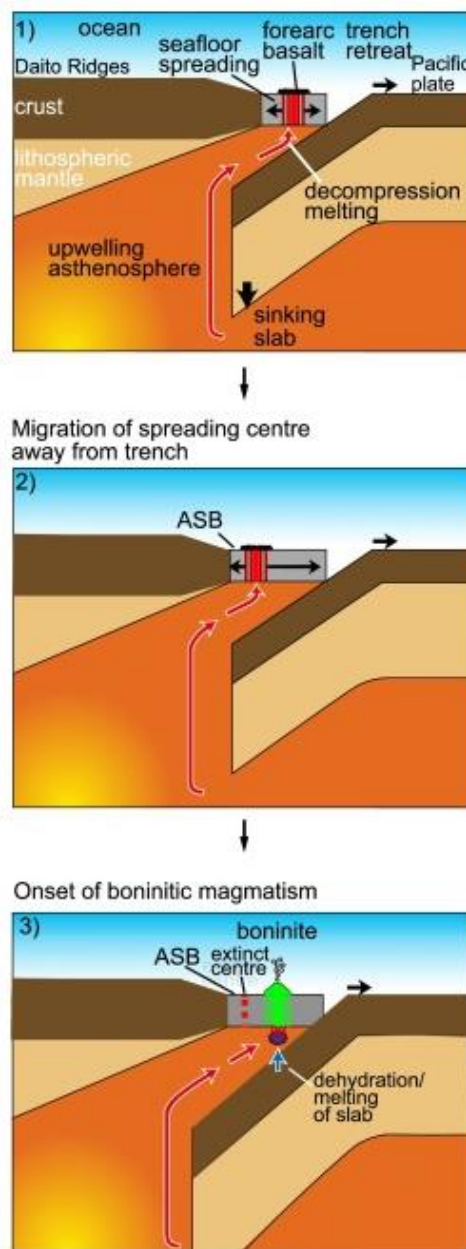


Figure 1. Schematic cartoon illustrating the evolution of the proto-IBM arc including formation of the ASB following subduction initiation. ASB formed from a migrating spreading centre associated with subduction initiation.

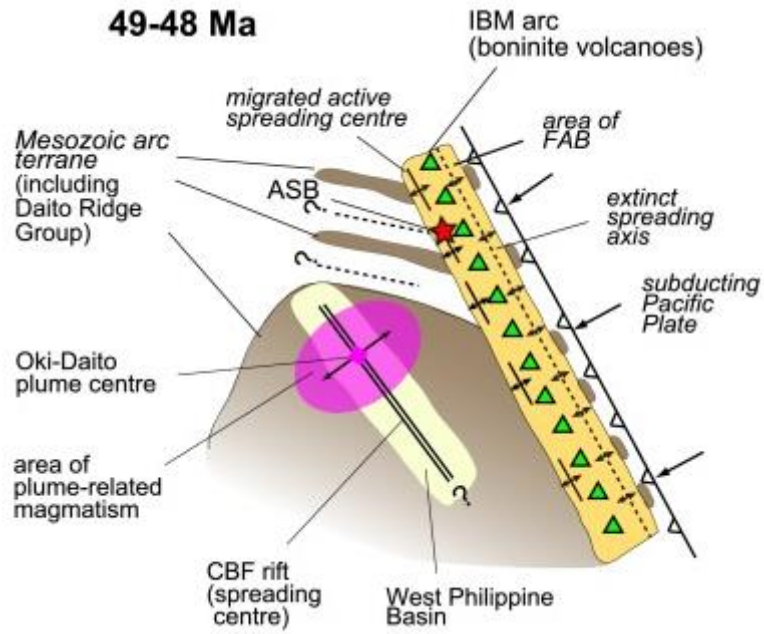


Figure 2. Schematic diagram showing a tectonic reconstruction of the Philippine Sea Plate around 49–48 Ma. Seafloor spreading associated with subduction initiation formed ocean crust on the overriding plate mainly composed of Mesozoic arc terrane with intervening ocean basins. Boninite volcanoes and later island arc volcanoes formed on this ocean crust. Spreading of the West Philippine Basin commenced by this period, almost contemporaneously with onset of magmatism caused by arrival of Oki-Daito plume.